

# Angular distributions of projectiles following electron capture from $C_{60}$ by 2.5-keV $Ar^{8+}$

B. Walch, U. Thumm, M. Stöckli, and C. L. Cocke

*J. R. Macdonald Laboratory, Physics Department, Kansas State University, Manhattan, Kansas 66506-2604*

S. Klawikowski

*Physics Department, University of Wisconsin, Madison, Wisconsin 53607*

(Received 30 January 1998; revised manuscript received 27 April 1998)

Experimental measurements of the projectile angular distributions for 2.5-keV  $Ar^{8+}$  ions capturing one to five electrons from a gas-phase  $C_{60}$  target are presented. The number of captured electrons was determined by demanding a coincidence between the scattered projectile and a charge-state-analyzed intact  $C_{60}$  recoil ion. The results are compared to calculations based on a dynamical classical overbarrier model. Good agreement is obtained only if the influence on the projectile trajectory by the large polarizability of the  $C_{60}$  target is taken into account, thereby making the collective dielectric response of the cluster target observable in a scattering experiment. [S1050-2947(98)08108-6]

PACS number(s): 34.70.+e

## I. INTRODUCTION

The interaction of a highly charged ion with a  $C_{60}$  cluster lies intermediate between the interaction of the ion with a many-electron atom and that with a solid surface. The last two cases have been heavily studied over more than a decade [1–5], and several characteristics of the capture process are well established. The simplest physical description attributes the capture to an overbarrier transfer of the target electrons to the projectile system. For a many-electron atomic target, the transfer of successively more tightly bound electrons occurs at successively smaller impact parameters. Models based on this picture [6–8] have been remarkably successful in dealing with the process. When the target atom is replaced by a surface, a similar overbarrier transfer occurs, reminiscent of field ionization, beginning at a projectile-surface distance for which the reduction of the potential barrier allows the departure of electrons at the top of the Fermi sea. Since the solid target presents an infinite reservoir of loosely bound electrons with binding energies equal to the work function of the material, multiple electron transfer (a flow of electrons) dominates. A  $C_{60}$  target presents some characteristics of both targets. It is similar to the solid in that it presents a very large reservoir of electrons with nearly the same binding energies and thus the cross section for the transfer of many electrons falls only slowly with the number of electrons captured. It is similar to the ion-atom case in that the collision time is limited and the ‘‘hollow atom’’ formed in the capture process is not destroyed in the encounter but survives to deexcite far downstream. It is also similar to the ion-atom case in that an intact recoil ion often remains whose charge state can be used to determine the number of electrons initially removed from the target. These characteristics of the ion-cluster collision have been exploited by several groups in recent years to try to establish connections between our understanding of ion-atom and ion-surface collisions [9–23].

Over the past five years it has become fairly well established that, for impact parameters large compared to the radius of  $C_{60}$ , the overbarrier model gives the correct picture of the transfer, even though details of the best specific for-

mulation of the model remain under investigation. For very slow projectiles, ionization of the target occurs slowly with a minimum of transfer of electronic energy, leaving the  $C_{60}$  vibrationally and electronically cold, with a high probability of surviving the ionization intact. Walch *et al.* [9] showed that  $C_{60}^{i+}$  up to  $i=6$  could be produced in this manner for slow  $Ar^{8+}$  ions on  $C_{60}$ , and established that the relevant impact parameters for such a collision lie in the range of 10 to 30 a.u. typically. Jin *et al.* [12] used a more highly charged projectile,  $Bi^{44+}$ , to produce  $C_{60}^{9+}$ , the most highly charged free  $C_{60}^{i+}$  ion reported to date. For charge states  $i < 9$ , Jin *et al.* found  $C_{60}^{i+}$  ion to have lifetimes of at least 5  $\mu$ sec. Thumm and co-workers [24–28] have developed a dynamic overbarrier/lifetimes model (DOBM) for the description of the electron transfer process, and applied it to the analysis of several observables. Bárány and co-workers [8,28] developed a multipole expansion of the ion- $C_{60}$  potential for application to collisions. Application of this model to electron transfer between multiply charged ions and  $C_{60}$  and between  $C_{60}$  targets and projectiles suggested that the charge left on the target  $C_{60}$  cage by electron removal may not be uniformly distributed on the cage surface (and therefore be thought of as localized at the center of the cage), as was assumed in the model of Thumm [24], but localizes near the surface [15]. Energy-gain measurements by Selberg *et al.* [13] showed distinct peaks in the energy-gain spectrum that could be attributed to discrete numbers of electrons removed from the target, and used a combination of energy gain and cross section to deduce that the charge removed from the  $C_{60}$  is, at least initially, localized near the point of emission. They also concluded that this charge redistributes quickly following the initial electron emission on a time scale short compared to the overall collision time. A recent quantitative analysis of these results was made by Thumm *et al.* using the DOBM [28].

In this paper we address the question of the trajectory followed by the projectile during this large-impact-parameter capture process by measuring the angular distribution of the capture products. Because the polarizability of  $C_{60}$  is huge, being about two orders of magnitude larger than typical

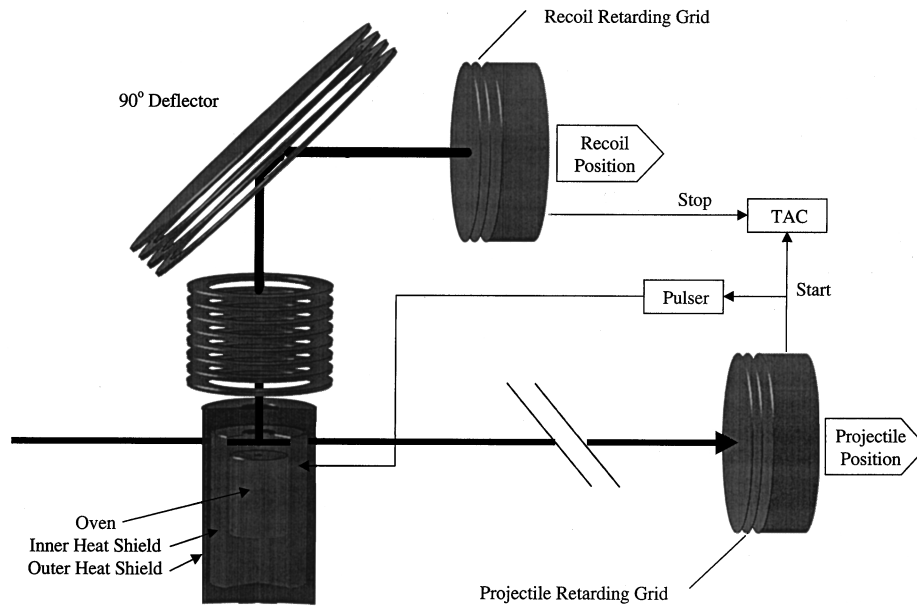


FIG. 1. Experimental setup.

atomic polarizabilities, it was expected that effects on the angular distributions due to the polarization interaction between projectile and target could be seen. This effect is similar to the image-charge acceleration seen when highly charged ions approach solids [5,29], except that the effect is not truncated by neutralization in collisions with  $C_{60}$  as it is in the solid collision case.

## II. EXPERIMENT

It is well established that the number of electrons captured from a many-electron target cannot be deduced from the final charge state of the projectile, since the capture occurs into multiply excited states of the projectile that relax by Auger electron emission before the projectile is analyzed. Briand *et al.* [11] found that the capture of any number of electrons by  $Ar^{17+}$  from  $C_{60}$  usually resulted in the retention by the projectile of only one of these. In general, the more loosely bound the target electrons are, the higher the  $n$  into which the projectile captures them and the more likely they are to be lost in the subsequent Auger relaxation. For the present experiment, this means that measurement of the projectile charge is unimportant, but that measurement of the recoil  $C_{60}$  charge is essential, since the charge state of the recoil gives the number of electrons captured.

We have done this using the apparatus shown in Fig. 1. An  $Ar^{8+}$  beam was extracted from the KSU EBIS, decelerated to a total energy of 2.5 keV, collimated to a small angular divergence, and directed through a beam of  $C_{60}$  produced by thermal effusion from a  $C_{60}$  (99.5% pure  $C_{60}$ ) oven. Recoil  $C_{60}$  ions and charged fragments were accelerated out of the interaction region by a pulsed electric field of 239 V/cm. This field was applied over a 5-mm gap for 1  $\mu$ sec. Following this extraction the recoil ions were further accelerated by a dc voltage over a distance of 9 cm through a total potential difference of 2 kV. They were then reflected by a 90° electrostatic mirror, and detected by a two-dimensional position-sensitive channel plate detector

(2DPSD). The ions were accelerated through a total potential drop of only 2 kV before detection, which is quite insufficient to ensure equal efficiencies for detection of all recoil charge states. Thus only relative angular distributions were measured for each final  $C_{60}$  charge state. (Absolute cross sections for 80-keV  $Ar^{8+}$  on  $C_{60}$  can be obtained from Refs. [9, 24, 26].) The use of the 90° reflector decreased the background counts in the recoil detector, which otherwise would have a direct view of the  $C_{60}$  oven. The projectile ions continued downstream a distance of 0.75 m onto the face of a second 2DPSD equipped with a retarding grid. The voltage of this grid was set to reject the main 8+ beam but admit charge states 7+ and lower. The recoil extraction field was pulsed, using as trigger the detection of the charge-changed projectile. The flight time between detection of the projectile and of the recoil  $C_{60}$  ion was used to determine the charge state of the recoil. The data were taken in event mode, which allowed off-line selection of the recoil charge state from the time-of-flight spectrum and exclusion of considerable background by selection of the recoil position on the recoil detector. The angular resolution function, determined by the width of the direct beam on the projectile detector, was measured to be 2.3 mrad, full width at half maximum (FWHM).

## III. THEORY

The DOBM was used to calculate angular distributions for the experiment described in the previous section. In this section, we outline the DCOM for soft ion-cluster collisions. For a more detailed description of this model, we refer to earlier publications [24–28]. During the ion-cluster interaction, energy levels, level occupations, transition rates, and total charges of target and projectile vary as a function of  $R$ , the distance between the centers of mass of target and projectile. In order to be transferred, the active electron is required to overcome the potential barrier  $V_B$  between target and projectile that is formed by the total electronic potential

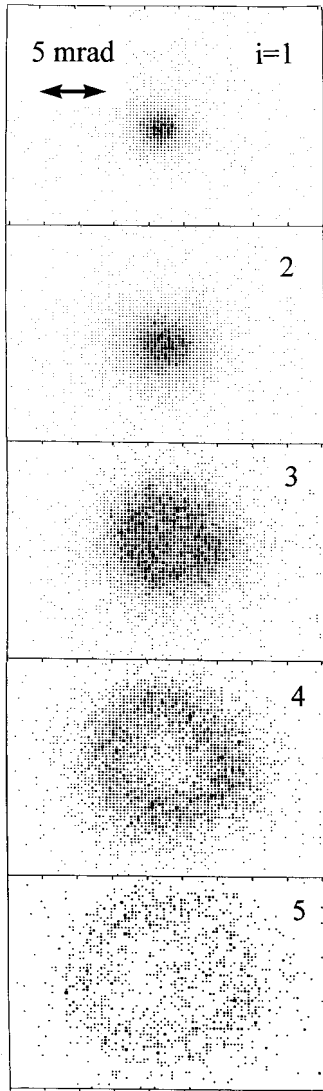


FIG. 2. Density plots of events on the projectile detector for 2.5-keV  $\text{Ar}^{8+}$  on  $\text{C}_{60}$ . The angular scale is indicated by a double-headed arrow. Each distribution was taken in coincidence with a detected  $\text{C}_{60}^{i+}$  ion, where  $i$  is indicated in the figure.

$$V(q_p, q_t, R, z) = -\frac{q_p}{|R-z|} - \frac{q_t}{z} + V_{\text{im}}(q_p, R, z), \quad (1)$$

where  $q_p$  and  $q_t$  are the charges of projectile and target acting on the electron in transition. The electron coordinate along the ‘‘internuclear axis’’ is denoted by  $z$ . The image potential  $V_{\text{im}}$  includes the active electron’s interaction with its own image charge and with the image of the effective projectile charge  $q_p$  in the target. For the purpose of representing classical image potentials as simple analytical expressions, we modeled  $\text{C}_{60}$  as a conducting sphere of radius  $a = \alpha^{1/3} = 8.52$  a.u. [9,10,24], where  $\alpha = 618$  a.u. is the static polarizability of the cluster [30].

As the projectile approaches the target, the first resonant transfer of an electron becomes possible at the distance  $R_1^*$ , when  $V_B$  energetically moves below the highest occupied target level. Similarly, as  $R$  continues to decrease, a second, third, etc. electron may be captured at critical distances  $R_2^* > R_3^* > \dots$  on the incoming trajectory.

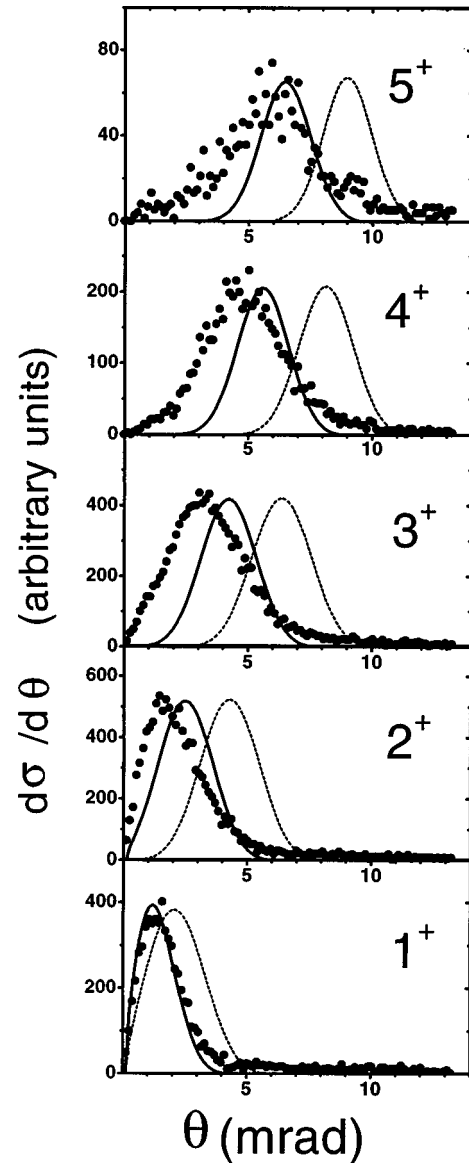


FIG. 3. Angular scattering distributions presented as  $d\sigma/d\theta$  for 2.5-keV  $\text{Ar}^{8+}$  on  $\text{C}_{60}$ . Filled circles: experimental data obtained by integrating the data of Fig. 2 over azimuthal angle; the charge state of the remaining  $\text{C}_{60}$  recoil,  $i+$ , is denoted on each figure. Solid line: theory, including image potentials. Dashed line: theory without image potentials.

We describe the projectile within an independent electron approach based on hydrogenic shells  $n$  with energy levels, occupation numbers, and degeneracies denoted by  $\epsilon_n^e(R)$ ,  $a_n(R)$ , and  $A_n = 2n^2$ . We do not resolve angular momentum sublevels. During the collision, projectile energy levels shift due to image-charge effects, Stark shifts induced by a charged target, and the dynamical change in screening induced by varying level populations. Target energy levels  $\epsilon_m^t(R)$  are shifted downward in the electric field of the positive projectile. After the capture of target electrons, positive charge accumulates on the target, which results in an additional downward shift of the target and projectile spectra.

The time evolution of the occupations  $a_n(t)$  and  $b_m(t)$  of projectile shells  $n$  and target levels  $m$  are obtained by integrating classical rate equations of the form

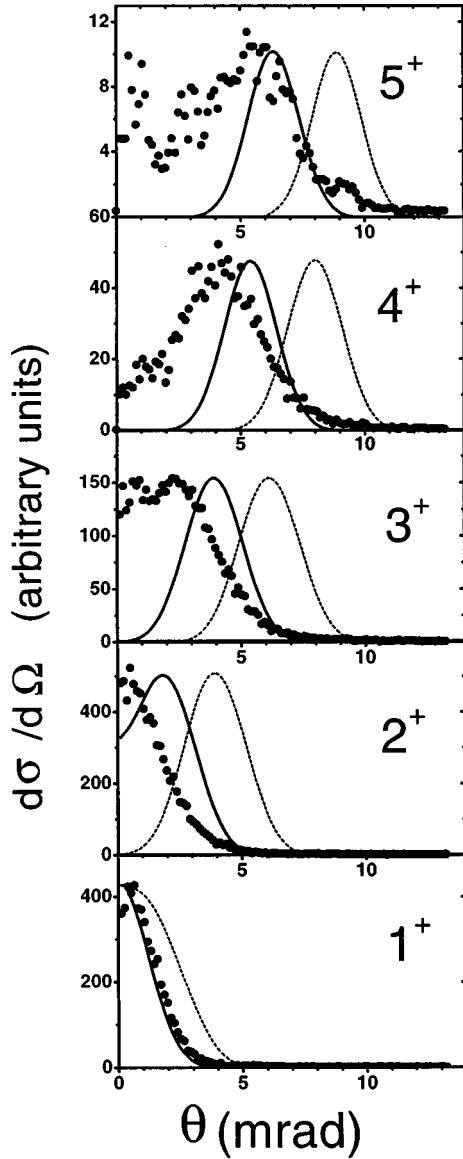


FIG. 4. Similar to Fig. 3, but presented as  $d\sigma/d\Omega$ .

$$\frac{d}{dt}a_n = \Gamma_{RN} - \Gamma_{RL}a_n + \sum_{n'>n} \Gamma_{n',n} - 2 \sum_{n'<n} \Gamma_{n,n'}, \quad (2)$$

$$\frac{d}{dt}b_m = \Gamma_{RL} - \Gamma_{RN}, \quad (3)$$

subject to the known initial occupations of projectile and target,  $a_n^0$  and  $b_m^0$ . Analytical expressions for the resonant-capture rates  $\Gamma_{RN}$  and resonant-loss rates  $\Gamma_{RL}$  are derived in Ref. [24] as classical transfer currents. All rates and occupation numbers implicitly depend on  $R(t)$ , and the above rate equations are solved simultaneously with Newton's equation for the projectile motion. The classical motion of the projectile, and hence the deflection angle, is determined by the competition between the repulsive dynamic Coulomb force between target and projectile and the attractive projectile self-image force. The electronic dynamics as given in the rate equations (2) and (3) influence the projectile motion through the time-dependent net charges of projectile and target in the dynamic Coulomb and self-image forces. In the

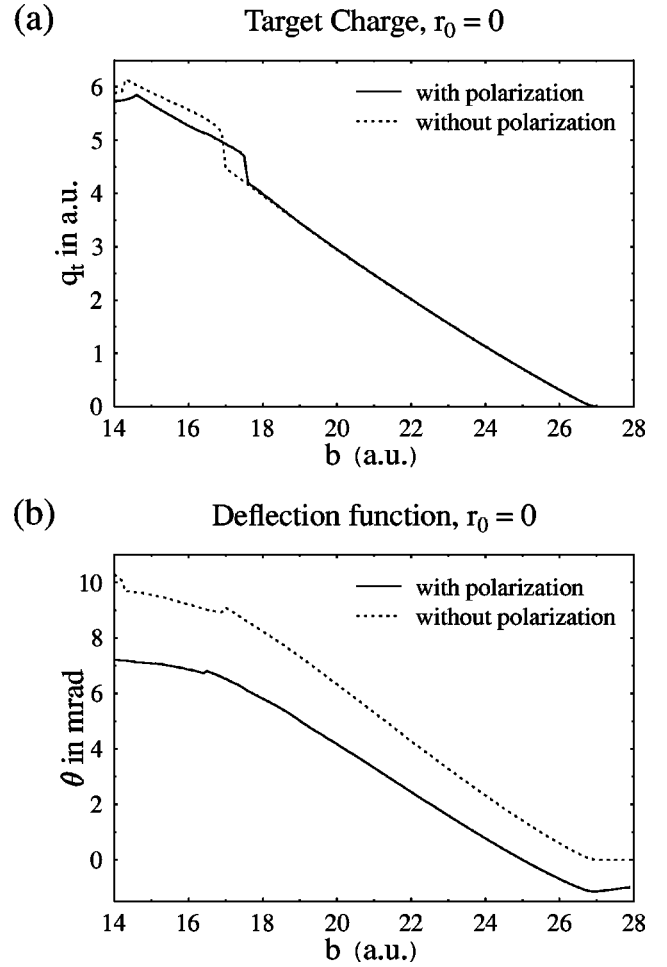


FIG. 5. Simulated final target charge states (a) and projectile deflection angles (b) in 2.5-keV  $\text{Ar}^{8+}$  on  $\text{C}_{60}$  collisions. Results “with” and “without” polarization refer to the inclusion (omission) of induced polarization interactions (see text).

two last terms of Eq. (2) we include fast Auger transitions for which the two active electrons start in the same shell, and which partly relax a multiply excited projectile while competing resonant electron transfer occurs. We model these fast transitions according to Ref. [5] and include statistical weights in the Auger transition rates  $\Gamma_{n_1,n_2}$  to take into account the number of electrons in the initial and final active shells. For a more detailed discussion of the projectile Auger relaxation rates we refer to Ref. [27]. Slow Auger relaxation channels are not included as they can be neglected *during* the collision. These transitions have a very small influence on the projectile deflection since the emission of these slow electrons occurs after the projectile has left the vicinity of the  $\text{C}_{60}$  and results in small and isotropic momentum transfers to the recoiling projectile.

We use the results of a self-consistent Dirac–Fock–Slater (DFS) calculation [26] in order to model the ground-state electronic structure of  $\text{C}_{60}$  and its positive ions  $\text{C}_{60}^{+i}$  with  $i \leq 7$ . This electronic structure calculation is based on a molecular-orbital linear combination of atomic orbitals (MO-LCAO) expansion scheme, which uses the  $2s$ ,  $2p_{1/2}$ , and  $2p_{3/2}$  atomic orbitals of C and bond distances of 2.772 and 2.561 a.u. between the C atoms. It yields the DFS single-particle energies of  $\text{C}_{60}^{+i}$  for charge states  $i=0,\dots,7$  and the

sequence of ionization potentials  $I_{i=1,\dots,7}=7.24, 10.63, 14.01, 17.44, 20.78, 24.24, \text{ and } 27.54$  eV, in good agreement with other calculated and experimental data ([26] and references therein).

We note that an interesting alternative effort to model scattering distributions for capture from  $C_{60}$  has been made by Sakurai [31] by using approximated Landau-Zener transition rates and classical potential scattering theory.

#### IV. RESULTS AND DISCUSSION

Figure 2 shows the position spectra from the projectile detector, gated on the TAC spectrum to isolate capture in which  $C_{60}^{i+}$  ( $i=1-5$ ) ions were created. Randoms and background have been subtracted from these spectra. The capture of increasing numbers of electrons results in successively larger scattering angles, with clear “donut” shapes appearing for the highest charge states. In Figs. 3 and 4 we show angular distributions obtained from integrating the density spectra of Fig. 2 over the azimuthal angle. In Fig. 3 the data are plotted as  $d\sigma/d\Omega$  versus  $\theta$ , where  $\theta$  is the projectile scattering angle. The resolution function, approximately a Gaussian in  $d\sigma/d\Omega$  with a FWHM of 2.3 mrad, is only slightly narrower in FWHM than is a plot of  $d\sigma/d\Omega$  for the 1+ recoils. While the resolution function dominates for the 1+ spectrum, it does not hide the true angular distribution for higher charge states. Figure 4 shows the same data plotted as  $d\sigma/d\theta$ , which gives a better picture of the angular weighting of the cross section but which hides somewhat the influence of the angular resolution function for the lowest two recoil charge states.

Deflection functions with and without the full image charge potential between projectile and the  $C_{60}$  are shown in Fig. 5. Corresponding angular distributions are plotted as full and dashed continuous lines in Figs. 3 and 4. In calculating the model angular distributions we have used, as a source function for each charge state  $i$ , an angular distribution uniformly spread between the angles at which a charge of  $(i + 1/2)$  units and  $(i - 1/2)$  units has left the target by the end of the collision (when the projectile is 100 a.u. downstream). Each source function was then folded with the experimental resolution function. The theoretical results have been normalized to approximately match the experimental peak heights. The agreement between model and experiment is rather good, especially for the lowest and highest recoil

charge states. In particular, the model without the image charge, or equivalently without taking into account the large polarizability of the  $C_{60}$ , would completely disagree with the data for  $i=1+$  and  $5+$ , while the agreement is good when the image charge is taken into account. The model predicts that the  $d\sigma/d\Omega$  distribution for  $i=1+$  is nearly a delta function at zero degrees, in agreement with experiment, while ignoring the image charge predicts a larger scattering angle, quite excluded by experiment. The DCOM predicts that the production of any given charge state occurs over a narrow slice in impact parameter, and thus generates very localized peaks in  $d\sigma/d\theta$ . This is not seen in the measured data presented in this paper. However, the impact parameter intervals are also related to capture cross sections that were recently found to agree with experiment within the expected accuracies of measurement and simulation [22,24,26].

#### V. CONCLUSIONS

The very close agreement between the DOBM and the angular distributions presented here confirm the picture of large-impact-parameter capture from  $C_{60}$  as an overbarrier process very similar to the corresponding processes in both ion-atom and ion-surface collisions. Through the use of deflection functions based on this model, it should be possible to experimentally control the impact parameter for such collisions. This provides the experimentalist with a new parameter for the study of the extraction of electrons from solidlike targets as a function of the distance of closest approach to the (curved) surface. It also allows the investigation of questions such as how close the projectile can pass without disintegrating the  $C_{60}$  cage, which is closely related to the question of how much total energy is transferred to the  $C_{60}$  internal degrees of freedom as a function of impact parameter. Furthermore, the pronounced influence of the target polarizability on the projectile deflection points to future refined investigations of the dielectric response of many-electron targets by measuring scattering distributions in recoil coincidence experiments.

#### ACKNOWLEDGMENT

This work was supported by the Division of Chemical Sciences, Basic Energy Sciences, Office of Energy Research, U.S. Department of Energy.

- 
- [1] M. Barat and P. Roncin, *J. Phys. B* **25**, 2205 (1992).
  - [2] E. K. Janev and H. Winter, *Phys. Rep.* **117**, 265 (1985).
  - [3] E. K. Janev and L. P. Presnyakov, *Phys. Rep.* **70**, 1 (1981).
  - [4] C. L. Cocke, in *Review of Fundamental Processes and Applications of Atoms and Ions*, edited by C. D. Lin (World Scientific, Singapore, 1993), p. 111.
  - [5] J. Burgdörfer, in *Review of Fundamental Processes and Applications of Atoms and Ions* (Ref. [4]), p. 517.
  - [6] H. Ryufuku, K. Sasaki, and T. Watanabe, *Phys. Rev. A* **21**, 745 (1980).
  - [7] A. Niehaus, *J. Phys. B* **19**, 2925 (1986).
  - [8] A. Bárány, in *Proceedings of the XVI International Conference on the Physics of Electronic and Atomic Collisions*, edited by A. Dalgarno, R. S. Freund, P. M. Koch, M. S. Lubell, and T. B. Lucatorto, AIP Conf. Proc. No. 205 (AIP, New York, 1990), p. 246.
  - [9] B. Walch, C. L. Cocke, R. Voelpel, and E. Salzborn, *Phys. Rev. Lett.* **72**, 1439 (1994).
  - [10] A. Bárány and C. J. Setterlind, *Nucl. Instrum. Methods Phys. Res. B* **98**, 184 (1995).
  - [11] J. P. Briand, B. d’Etat-Ban, D. Schneider, M. A. Briere, V. Decaux, J. W. McDonald, and S. Bardin, *Phys. Rev. A* **53**, 2194 (1996).
  - [12] J. Jin, H. Khemliche, M. H. Prior, and Z. Xie, *Phys. Rev. A* **53**, 615 (1996).
  - [13] N. Selberg, A. Bárány, C. Diedermaun, C. J. Setterlind, H.

- Cederquist, A. Langereis, M. O. Larsson, A. Wannstrom, and P. Hvelplund, *Phys. Rev. A* **53**, 874 (1996).
- [14] T. LeBrun, H. G. Berry, S. Cheng, R. W. Dunford, H. Evensen, D. S. Gemmel, and E. P. Kanter, *Phys. Rev. Lett.* **72**, 3965 (1994).
- [15] H. Shen, P. Hvelplund, B. Mathur, A. Barany, H. Cederquist, N. Selberg, and D. Lorents, *Phys. Rev. A* **52**, 3847 (1995).
- [16] V. V. Afrosimov, A. A. Basalaev, V. P. Belik, Yu. V. Naide, M. N. Panov, and O. V. Smirnov (unpublished).
- [17] C. J. Setterlind, P. Sakurai, and A. Barany (unpublished).
- [18] T. Schlatholter, R. Hoekstra, and R. Morgenstern (unpublished).
- [19] J. Opitz, M. Benndorf, U. Wemer, U. Brinkmann, and B. A. Huber (unpublished).
- [20] J. Bernard, L. Chen, A. Denis, J. Desesquelles, and S. Martin, *Phys. Scr.* **T73**, 291 (1997).
- [21] A. Itoh, H. Tsuchida, K. Miyabe, M. Imai, and N. Imanishi, *Phys. Scr.* **T73**, 289 (1997).
- [22] B. A. Huber (unpublished).
- [23] A. Barany (unpublished).
- [24] U. Thumm, *J. Phys. B* **27**, 3515 (1994). In this reference, a factor 1/2 is not printed in the self-image potentials. This factor, however, was included in all computations. In addition, the present work uses a different sign convention in the definition of interaction potentials.
- [25] U. Thumm, *J. Phys. B* **28**, 91 (1995).
- [26] U. Thumm, T. Bastug, and B. Fricke, *Phys. Rev. A* **52**, 2955 (1995).
- [27] U. Thumm, *Phys. Rev. A* **55**, 479 (1997).
- [28] U. Thumm, A. Barany, H. Cederquist, L. Hagg, and C. J. Setterlind, *Phys. Rev. A* **56**, 4799 (1997).
- [29] H. Winter, *Europhys. Lett.* **18**, 207 (1992).
- [30] M. J. Puska and R. M. Nieminen, *Phys. Rev. A* **47**, 1181 (1993).
- [31] P. Sakurai, M.Sc. thesis, Univ. Stockholm, 1997 (unpublished).